Preprints of the 21st IFAC World Congress (Virtual)
Berlin, Germany, July 12-17, 2020

Subterranean MAV Navigation based on Nonlinear MPC with Collision Avoidance Constraints ⋆

Sina Sharif Mansouri * **Christoforos Kanellakis** * **Emil Fresk** **
Björn Lindqvist * **Dariusz Kominiak** * **Anton Koval** *
Pantelis Sopasakis *** **George Nikolakopoulos** *

* *Robotics Team, Department of Computer, Electrical and Space Engineering, Luleå University of Technology, Luleå SE-97187, Sweden.*
** *WideFind AB, Aurorum 1C, Luleå SE-97775, Sweden*
*** *School of Electronics, Electrical Engineering and Computer Science (EEECS), Queen's University Belfast and Centre for Intelligent Autonomous Manufacturing Systems (i-AMS), United Kingdom*

Abstract: Micro Aerial Vehicles (MAVs) navigation in subterranean environments is gaining attention in the field of aerial robotics, however there are still multiple challenges for collision free navigation in such harsh environments. This article proposes a novel baseline solution for collision free navigation with Nonlinear Model Predictive Control (NMPC). In the proposed method, the MAV is considered as a floating object, where the velocities on the x, y axes and the position on altitude are the references for the NMPC to navigate along the tunnel, while the NMPC avoids the collision by considering kinematics of the obstacles based on measurements from a 2D lidar. Moreover, a novel approach for correcting the heading of the MAV towards the center of the mine tunnel is proposed, while the efficacy of the suggested framework has been evaluated in multiple field trials in an underground mine in Sweden.

Keywords: NMPC, Collision Avoidance, Subterranean, MAV, Autonomous Tunnel Inspection, Mining Aerial Robotics

1. INTRODUCTION

Recent technological developments in Micro Aerial Vehicles (MAVs) has resulted to a rapid growth of the usage of these platforms in different challenging applications, such as underground mine inspection (Mansouri et al., 2020, 2019), infrastructure inspection Mansouri et al. (2018) and subterranean exploration (Rogers et al., 2017). These platforms explore the area and provide access to unreachable, complex, dark and dangerous locations, while minimizing the human involvement in service and inspection procedures.

Navigation of aerial robots in underground mine tunnels should cope with multiple challenges as conditions, such as the lack of illumination, narrow passages, crossing paths, limited entrances, dust, high moisture and uneven surfaces directly affect the reliability of sensor measurements and thus the MAV requires a collision avoidance method. Figure 1 shows photos from one underground mine in Sweden to indicate these conditions in different mine locations. This work addresses the autonomous navigation from a novel perspective by using the concept of a floating object, where the method does not not rely on global information and position estimation, and the dependency on high end and highly expensive sensors is removed. The proposed system, from an application point of view, fits in scenarios towards autonomous underground mine inspection schemes.

This work proposes a low-cost and resource-constrained platform for navigation and collision avoidance in underground tunnels. The proposed method considers x, y-velocities and altitude and attitude estimation, instead of a full pose estimation. The Nonlinear Model Predictive Control (NMPC) is implemented for following the velocities and the altitude references, while considering the dynamics of the platform and avoiding obstacles, based on the measurements from a 2D lidar.

The NMPC optimization problem is solved using OpEn (Sopasakis et al., 2020), which is an open-source solver written in Rust: a fast modern programming language, which offers memory safety guarantees, an important feature for embedded applications. Furthermore, OpEn implements the proximal averaged Newton-type method for optimal control Proximal Averaged Newton-type method for Optimal Control (PANOC) (Sathya et al., 2018), combined with the quadratic penalty method (Hermans et al., 2018) to accommodate nonlinear constraints.

Moreover, a weighted arithmetic mean based on 2D lidar measurements is implemented to correct the heading of the MAV towards open areas. To the best of our knowledge, this is the first work on embedded NMPC with the concept

⋆ This work has been partially funded by the European Unions Horizon 2020 Research and Innovation Programme under the Grant Agreement No. 730302 SIMS. Corresponding author's e-mail: sinsha@ltu.se

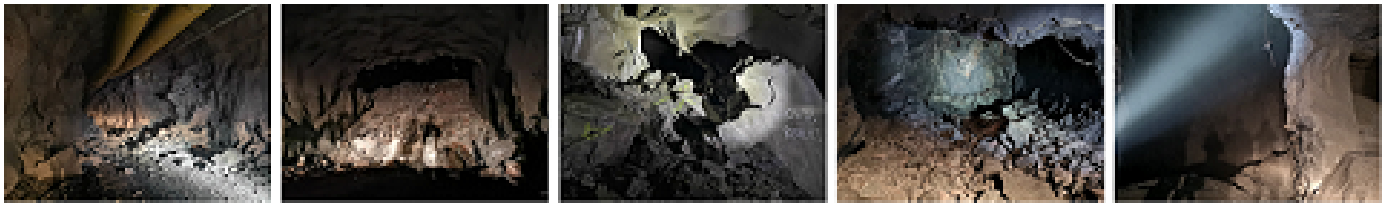

Fig. 1. Few examples of underground mine environments with limited access and obstacles that shows the need for collision avoidance methods for MAV navigation.

of floating objects and collision avoidance for underground mine navigation.

1.1 Background & Motivation

MAV autonomous navigation (Nieuwenhuisen and Behnke, 2016) with collision avoidance in unknown complex indoor and GPS-denied environments essentially relies on how precise perception of the environment is. There are many works that address this challenging task (Lu et al., 2018), mainly focusing on visual and range finding approaches.

Visual or camera-based approaches can provide rich information about the environment, while being relatively lightweight and cheap. There is a lot of research behind MAV camera-based autonomous navigation. For instance, in (Shen et al., 2012) an algorithm is proposed with collision avoidance, which determines regions for further exploration based on the evolution of a stochastic differential equation. Another approach (Bircher et al., 2016) for the path generation utilizes a receding horizon path planning algorithm, which acquires visual information from the sensing system and provides a map of the explored environment for collision free navigation and for tracking exploration progress. In (Al-Kaff et al., 2017) the authors propose an algorithm that uses feature points for obstacle detection and by further estimating their positions via the visual data the MAV takes the avoidance action. These approaches are based on processing visual information, which reduces map uncertainty and allows obstacle avoidance. However, camera-based approaches typically require well-illuminated environments and high computation power to process visual information for localization, to store the previous position and to calculate the next position, while avoiding revisiting known areas. Additionally the collision avoidance system strongly relies on a map, which can drift or camera, which has limited Field of View (FoV) and it may result in collision with obstacles. These shortcomings make visual approaches hardly applicable in dark, harsh and large environments.

Range finding approaches provide distances to objects in its FoV and strongly rely on the quality of the metric data. Among a large number of sensors, lidar or laser rangefinder is presently a standard sensor for mobile robotics applications. In the field trials with the MAV some works address navigation and collision avoidance tasks based on lidars, such as autonomous MAV inspection inside buildings for maintenance or disaster management (Droeschel et al., 2016), aerial structure inspection in the outdoor scenario (Azevedo et al., 2017), indoor chimney inspection (Quenzel et al., 2019), etc. All these approaches rely on reactive navigation schemes like potential fields Kanellakis et al. (2018) or occupancy grid maps (such as graph-search methods). The main disadvantages of these schemes lie in local optima, limiting their ability to find their way around obstacles without a global planner, and tuning parameters for attractive and repulsive forces for different environments, while the limitation of the map based approaches are the same as discussed above.

There are few works that consider the navigation problem in dark tunnels, such as (Özaslan et al., 2017). In this work the authors address estimation, control, navigation and mapping problems for autonomous tunnel inspection using MAVs validating their approach with field trials. However, the use of a high-end sensor suit limits the applicability of the overall method. In (Bharadwaj et al., 2016) the authors proposed an infrared camera for navigation in dark environments, however the work doesn't provide autonomous navigation of the MAV. In (Dang et al., 2019) the approach for autonomous aerial navigation in a subterranean environment is proposed, while the method is evaluated in underground tunnels. The approach relied on the global planner and a high end sensor for collision avoidance. This results to collision in case of drifts in the map and the MAV should have a low-level collision avoidance scheme. In (Huang et al., 2019) autonomous blimp Duckiefloat is proposed for tunnel navigation, however collision avoidance is not considered due to non-rigid body of the platform and it is collision-tolerant.

1.2 Contributions

The first and major contribution of this article is the development of the MAV as a floating object, while not relying on full odometry information. As position information drifts over time, especially in harsh environments, such as mines with dust, low illumination, wet surfaces, etc. In the worse case scenario, this may result in failure of the mission or collision of the platform. The proposed method can be used as a baseline controller that guarantees collision free navigation based on local information, while a higher level controller can be used for generating reference velocities based on a global map and exploration requirements.

The second contribution is the development and experimental validation of a lidar-based navigation system with collision avoidance capabilities using NMPC. The associated optimization problem is solved on an Aaeon UP-Board embedded platform onboard the MAV, using Rust code that is auto-generated using OpEn (Sopasakis et al., 2020).

The third contribution specifically highlights the heading command generation as the MAV has to identify the direction of the flight in the tunnel navigation task. To address this issue, this work proposes a geometry-based

approach to obtain the heading rate towards the open area, which is improved by integrating the gyro response for better robustness.

Finally, the fourth major contribution, stems from evaluating the performance of the proposed method in an underground mine located in Sweden. As it is presented the proposed method has a significant novelty and impact on embedded NMPC navigation with collision avoidance for underground tunnels. The following link https://youtu.be/-MP4Sn6Q1uo provides a video summary of the overall results.

1.3 Outline

The rest of the article is structured as follows. Initially the preliminaries are explained in Section 2, then the mathematical models of the MAV and the obstacles are described in Section 3. Next, a presentation of the NMPC formulation and the solver is described in Section 4. The geometry approach for generating heading rate commands is discussed in Section 5. Section 6 presents the hardware setup and provides the experimental results from the underground mine with uneven surfaces. Finally, Section 7 concludes the article by summarizing the findings and offering some directions for future research.

2. PRELIMINARIES

In this article, the main part to enable autonomous navigation is to consider the MAV as floating object, to remove dependencies on accurate localization schemes. Thus, the position estimation in x and y axes is not considered. The MAV is equipped with multiple sensor suits, such as onboard Inertial Measurement Unit (IMU) to estimate the attitude $[\phi, \theta]^\top$, an optical flow sensor for linear velocities $[v_x, v_y]^\top$, and one beam lidar for height z and v_z velocity estimation. Moreover, the 2D lidar provides a set of R ranges with r to denote the range generated at an angle of rotation ξ, with the angular resolution depend on the 2D lidar characteristics. The one beam lidar provides the distance to the ceiling d^{+z}. The main challenge of navigation is to avoid collision and extract a proper heading to follow an obstacle free path along the tunnels, while the position of the MAV is not known. This article proposes the novel approach and considers the kinematic of the obstacles in respect to the MAV, while no global information of obstacle positions is available.

3. MAV DYNAMICS AND OBSTACLE KINEMATICS

The MAV is considered as a six Degree of Freedom (DoF) object with a Body-Fixed Frame $\mathbb{B}$ attached and the inertial frame $\mathbb{E}$ as depicted in Figure 2. The MAV is modelled by the position of the center of the mass in the inertia frame and the orientation of the body around each axes with respect to the inertial frame (Kamel et al., 2017). This modelling requires a full state estimation for the position and orientation in the inertial frame. However, underground mines are Global Positioning System (GPS)-denied environments, IMU measurements are affected by accumulated errors and due to low illumination and lack of features, the performance of the vision based localization

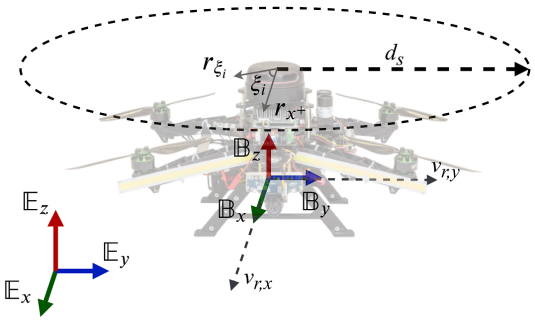

Fig. 2. Illustration of the MAV with the attached body fixed frame $\mathbb{B}$ and inertial frame $\mathbb{E}$, while the safety distance is shown by d_s, reference velocities by $v_{r,x}$, and $v_{r,y}$, lidar ranges by r and ξ is the angle correspond to the range.

methods, such as Visual Odometry (VO) (Balamurugan et al., 2016) is limited. Thus, in this article the MAV dynamics is defined in the body frame and does not depend on position estimation of the x and y-axes, to avoid affecting the performance of the controller by drifts and uncertainties in x, y positions. These drifts do not affect the proposed robust controller for collision avoidance either, while the MAV is modelled by (1) in body frame as:

$$\dot{z}(t) = v_z(t), \tag{1a}$$

$$\dot{v}(t) = R_{x,y}(\theta, \phi) \begin{bmatrix} 0 \\ 0 \\ T \end{bmatrix} + \begin{bmatrix} 0 \\ 0 \\ -g \end{bmatrix} - \begin{bmatrix} A_x & 0 & 0 \\ 0 & A_y & 0 \\ 0 & 0 & A_z \end{bmatrix} v(t), \tag{1b}$$

$$\dot{\phi}(t) = {}^1\!/_{\tau_\phi}(K_\phi \phi_d(t) - \phi(t)), \tag{1c}$$

$$\dot{\theta}(t) = {}^1\!/_{\tau_\theta}(K_\theta \theta_d(t) - \theta(t)), \tag{1d}$$

where $v = (v_x, v_y, v_z) \in \mathbb{R}^3$ is the vector of linear velocities, $\phi \in \mathbb{R} \cap [-\pi/2, \pi/2]$ and $\theta \in \mathbb{R} \cap [-\pi/2, \pi/2]$ are the roll and pitch angles, $R_{x,y}$ is the rotation matrix about the x and y axes, $T \in [0, 1]$ is the mass-normalized thrust, g is the gravitational acceleration, $A_x \in \mathbb{R}$, $A_y \in \mathbb{R}$, and $A_z \in \mathbb{R}$ are the normalized mass drag coefficients The low-level control system is approximated by first-order dynamics driven by the desired pitch and roll angles ϕ_d and θ_d with gains of $K_\phi, K_\theta \in \mathbb{R}^2$.

Additionally, five obstacles are considered for x^+, x^-, y^+, y^-, z^+ axes for collision avoidance in regards to the surroundings. These obstacles are modeled as surfaces perpendicular to the corresponding axes, while the distance of the surface d is the minimum range extracted from 2D lidar ranges in corresponding axes. The obstacle kinematics is presented by (2) in the body frame, where $\dot{d}$ is the velocity of the surface. As an example, the obstacle in the x axes has the $-v_x$ velocity compared to the MAV velocity in the body frame. In this approach, the distance to the obstacles can be predicted based on the MAV maneuvers.

$$\dot{d}^{x^+}(t) = -v_x(t), \tag{2a}$$

$$\dot{d}^{x^-}(t) = v_x(t), \tag{2b}$$

$$\dot{d}^{y^+}(t) = -v_y(t), \tag{2c}$$

$$\dot{d}^{y^-}(t) = v_y(t), \tag{2d}$$

$$\dot{d}^{z^+}(t) = -v_z(t). \tag{2e}$$

4. NONLINEAR MODEL PREDICTIVE CONTROL

In this article, the NMPC with collision avoidance constraints are developed and solved by PANOC (Sathya et al., 2018) to guarantee real-time performance. The NMPC objective is to generate attitude ϕ_d, θ_d and thrust commands T_d for the low-level controller, while the reference altitude and velocities $[z_r, v_{r,x}, v_{r,y}]^\top$ are provided from the operator. The Proportional Integral Derivative (PID) controller in the flight controller generates the motor commands $[n_1, \ldots, n_4]^\top$ for the MAV. A block diagram representation of the proposed NMPC and the corresponding low-level controller is shown in Figure 3.

Based on the non-linear dynamics of the MAV (1) and kinematics of the obstacles (2), the state of the system is $\boldsymbol{x} = [z, v_x, v_y, v_z, \phi, \theta, d^{x^+}, d^{x^-}, d^{y^+}, d^{y^-}, d^{z^+}]^\top$, $\hat{\boldsymbol{x}} = [\hat{z}, \hat{v_x}, \hat{v_y}, \hat{v_z}, \hat{\phi}, \hat{\theta}]^\top$ is the estimated state from Extended Kalman Filter (EKF) for MAV dynamics, while the distances to the surfaces are obtained from the 2D lidar range measurement, and the control input is: $u = [\phi_d, \theta_d, T]^\top$. By discretizing (1) with the Euler method and with a sampling time of T_s, we obtain a discrete-time dynamical system as:

$$\boldsymbol{x}_{t+1} = f(\boldsymbol{x}_t, u_t).$$

In the NMPC approach, at every time instant k, a finite-horizon problem with prediction horizon $N \in \mathbb{N}^{\geq 2}$ is solved, while $\boldsymbol{x}_{k+j|k}$, and $u_{k+j|k}$ are the states and control actions $k+j$ steps ahead of the current time step k. NMPC generates an optimal sequence of control actions $u^\star_{k|k}, \ldots, u^\star_{k+N-1|k}$ and the first control action $u^\star_{k|k}$ is applied to the flight controller using a zero-order hold element, that is, $u_t = u^\star_{k|k}$ for $t \in [kT_s, (k+1)T_s]$. For the proposed NMPC, the following finite horizon cost function is introduced:

$$J = \sum_{j=0}^{N-1} \underbrace{\|z_{k+j+1|k} - z_r\|^2_{Q_z}}_{\text{altitude error}} + \underbrace{\|v_{k+j+1|k} - v_r\|^2_{Q_v}}_{\text{velocity error}} + \underbrace{\|u_{k+j+1|k} - u_r\|^2_{Q_u}}_{\text{actuation}} + \underbrace{\|u_{k+j|k} - u_{k+j-1|k}\|^2_{Q_{\Delta u}}}_{\text{smoothness cost}}. \quad (3)$$

The first and second terms of J are the tracking of the desired altitude, and velocity references respectively. The third term is the hovering term, where u_{ref} is $[0, 0, g]^\top$, which is the hover thrust with horizontal angles. The forth term penalizes the aggressiveness of the obtained control actions. Additionally, $Q_z \in \mathbb{R}$, $Q_v \in \mathbb{R}^{3\times3}$, $Q_u \in \mathbb{R}^{3\times3}$, $Q_{\Delta u} \in \mathbb{R}^{3\times3}$ are the weights for each term of the objective function, which reflects the relative importance of each term.

Additionally, to avoid the obstacles, five constraints are defined in (4), while the NMPC predicts the distance of the obstacles based on the kinematic of the constraints (2)

$$d_s - d^{x^+}_{k+j|k} - \dot{d}^{x^+}_{k+j+1|k} T_s \leq 0, \quad (4a)$$
$$d_s - d^{x^-}_{k+j|k} - \dot{d}^{x^-}_{k+j+1|k} T_s \leq 0, \quad (4b)$$
$$d_s - d^{y^+}_{k+j|k} - \dot{d}^{y^+}_{k+j+1|k} T_s \leq 0, \quad (4c)$$
$$d_s - d^{y^-}_{k+j|k} - \dot{d}^{y^-}_{k+j+1|k} T_s \leq 0, \quad (4d)$$
$$d_s - d^{z^+}_{k+j|k} - \dot{d}^{z^+}_{k+j+1|k} T_s \leq 0, \quad (4e)$$

where d_s is the defined safety distance given by the operator. The proposed constraints guarantee that the MAV has at least d_s distance to each obstacle. The following optimization problem can be defined:

$$\underset{\{u_{k+j|k}\}_{j=0}^{N-1}}{\textbf{minimize}}\ J \quad (5a)$$
$$\textbf{subject to}: \boldsymbol{x}_{k+j+1|k} = f(\boldsymbol{x}_{k+j|k}, u_{k+j|k}), \quad (5b)$$
$$\text{Constraints (4)}, \quad (5c)$$
$$u_{k+j|k} \in [u_{\min}, u_{\max}], \quad (5d)$$

for $j = 0, \ldots, N-1$.

Problem (5) is a parametric non-convex optimization problem that must be solved online, by typical on-board computation platforms with limited computing resources and within the hard run-time requirements of the navigation controller. To that end, we use the fast and efficient optimization solver Optimization Engine (for short `OpEn`) developed by Sopasakis et al. (2020). `OpEn` can solve problems of the general form

$$\textbf{Minimize}_{u\in U}\ \ell(u), \quad (6a)$$
$$\textbf{subject to}: F(u) = 0, \quad (6b)$$

by means of the penalty method and PANOC. The solver allows the designer to provide the problem specification in Python and generates code written in Rust (`https://rust-lang.org`): a fast programming language that guarantees safe memory management. This is an important desideratum for safety-critical applications such as MAV navigation. In order to write Problem (5) in the form of (6), we first eliminate the state sequence following the procedure detailed in (Sathya et al., 2018). This way, we have a problem of the decision variable $u = (u_{k|k}, u_{k+1|k}, \ldots, u_{k+N-1|k}) \in \mathbb{R}^{3N}$, which is constrained in $U = [u_{\min}, u_{\max}]^N$. Constraint (4a) is equivalent to

$$\max\left\{0, d_s - d^{x^+}_{k+j|k} - \dot{d}^{x^+}_{k+j+1|k} T_s\right\} = 0. \quad (7)$$

Likewise, constraints (4) can all be written as equality constraints.

5. HEADING CORRECTION

The purpose of this module is to guide the MAV towards the direction that has the largest amount of navigable space. The 2D lidar provides range measurements for each degree of of rotation, thus the weighted arithmetic mean (Madansky and Alexander, 2017) is proposed. In the weighted arithmetic mean, the range value for each angle is used as a weight for the corresponding angle. The weighted arithmetic mean is calculated as:

$$\psi_k = \frac{\sum_i r_{i,k} \xi_i}{\sum_i r_{i,k}} \quad (8)$$

where $i \in [i_{min},\ i_{max}]$ is the set of beam angle indexes and r_i is the range measurement for each corresponding angle ξ

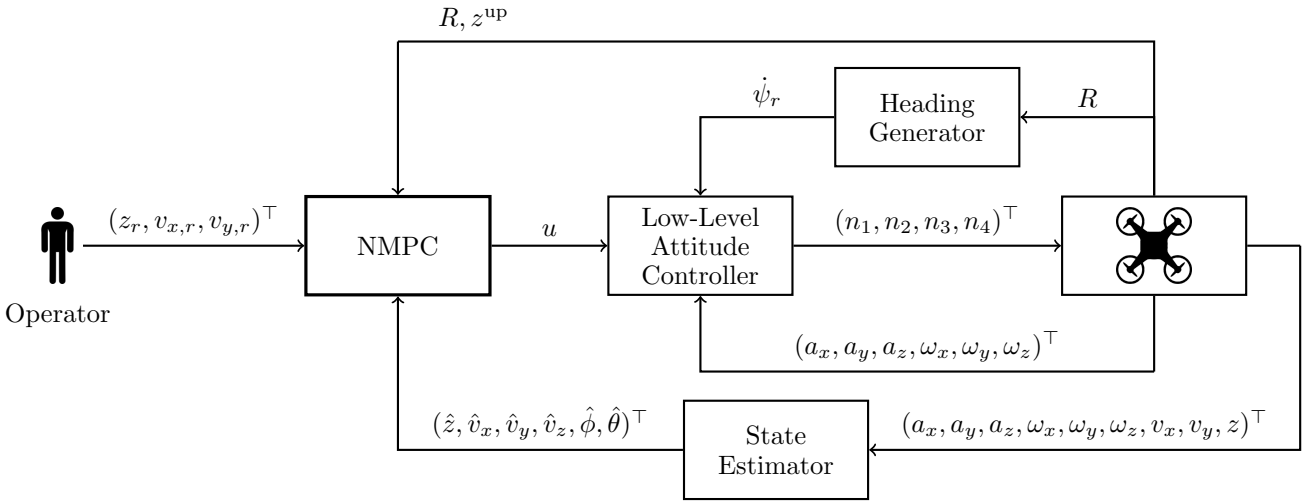

Fig. 3. Control scheme of the proposed navigation module, where the heading commands are provided from the geometry approach. The NMPC generates thrust and attitude commands, while the low level controller generates motor commands $[n_1, \ldots, n_4]^\top$. The velocity estimation is based on IMU measurements, optical flow and downwards facing single beam lidar.

of 2D lidar rotation. ξ_{min} and ξ_{max} define a range of angles, as shown in the Figure 2, and there are angles for y^+ and y^- axes in the body frame, thus the range measurements from y^- axis up to y^+, based on the right hand rule are used. However, this result is noisy and subject to spurious changes in the environment. For improving this, the integrated z-axis of the gyro in the IMU is used as a prior, using a complementary filter as follows.

Initially, the heading is integrated from the z-axis angular rate to predict the movement as:

$$\hat{\psi}_{k|k-1} = \hat{\psi}_{k-1|k-1} + \omega_{z,k} T_s, \tag{9}$$

which in the sequel is corrected using the estimated angle from the 2D lidar:

$$\hat{\psi}_{k|k} = \beta \hat{\psi}_{k|k-1} - (1-\beta)\psi_k, \tag{10}$$

where $\beta \in (0,\ 1)$ is a classic complementary filter, which was chosen due to its simplicity in tuning for generating robust results. It should be also noted the negation in the second term, $-(1-\beta)\psi_k$, that is generated from the fact that the measured free space always rotates with the inverted angular rates relative to the MAV.

The obtained heading angle is fed to the low level proportional controller with gain of $k_p > 0$ to always have the MAV point toward the open space:

$$\dot{\psi}_{r,k} = -k_p \hat{\psi}_{k|k}. \tag{11}$$

6. RESULTS

This section describes the experimental setup and the experimental evaluation that has been performed in an underground mine.
Link: https://youtu.be/-MP4Sn6Q1uo provides a video summary of the system.

6.1 Experimental Setup

In this work, a low-cost quad-copter that is developed at Luleå University of Technology has been operated in an underground mine. The developed platform is presented in (Mansouri et al., 2020), while the platform is equipped with an additional upwards facing single beam Lidar-lite v3 at 100 hz for measuring distance to the ceiling. Figure 4 depicts the platform highlighting the sensor suits and dimensions.

6.2 Experimental Evaluation

This work evaluates the method in two different types of environments; a tunnel environment and a tunnel blockage. This highlights the adaptability and feasibility of the methods in different scenarios in the underground mines. Two locations are selected for this purpose, the first location is an underground iron mine with strong magnetic fields, while the second one is underground tunnels without corrupting magnetic fields, both environments are located in Sweden. The first location has a width and height of approximately 6 m and 4 m with tunnels and blockage areas. The second location morphology resembled an S shape and the dimensions of the area, where the MAV navigates autonomously were 3.5(width) $\times$ 3(height) m^2. It should be highlighted that none of the flights resulted to a collision and the flights were terminated only due to battery drainage.

The tuning parameters of the NMPC and the parameters of the MAV model are presented in the Tables 1 and 2 correspondingly. The NMPC prediction horizon N is 40 and the control sampling time T_s is 0.05 s. The β and k_p for the heading generator approach are 0.95 and 0.03 respectively. During the navigation task the average solver time for the optimization framework is around 10ms, while it consumes an average of 10% of the CPU usage.

Tunnel Environment: The MAV is evaluated in the two tunnels with different dimensions. Figure 5 shows the tunnel environments, while the MAV performs autonomous flight with on-board lights.

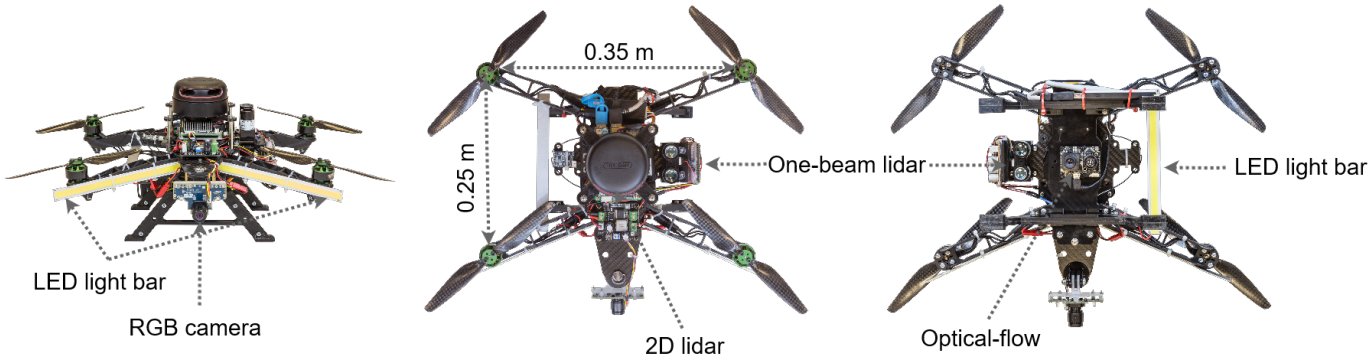

Fig. 4. The developed quad-copter equipped with a forward looking camera, a LED lights, optical flow, 2D lidar and single beam lidar looking upward and downward.

Table 1. The tuning parameters of the NMPC.

Q_z	Q_v	Q_u	$Q_{\Delta u}$	d_s
10	$[5,5,5]^\top$	$[20,20,20]^\top$	$[20,20,20]^\top$	1 m

T	ϕ_{min}	ϕ_{max}	θ_{min}	θ_{max}
$[0,1]\cap\mathbb{R}$	-0.4 rad/s	0.4 rad/s	-0.4 rad/s	0.4 rad/s

Table 2. The parameters of the MAV model.

g	A_x	A_y	A_z	K_ϕ	K_θ	τ_ϕ	τ_θ
9.8 m/s^2	0.1	0.1	0.2	1	1	0.5 s	0.5 s

Fig. 5. The tunnel environments, while the first and second locations are left and right pictures respectively.

Figure 6 shows the distances from the surroundings of the MAV in the first tunnel environment, where the d^{x^+}, d^{x^-}, d^{y^+}, d^{y^-}, d^{z^+} are distances to the corresponding body frame axes. In this test, the MAV autonomously navigates with $z_r = 1.0$ m, $v_{x,r} = 0.5$ m/s, $v_{y,r} = 0.0$ m/s. The maximum range of the used 2D lidar is 15 m, however it reports inf for ranges out of this bound or if the laser beam does not bounce back due to wet surfaces. In the following figures the inf values are not shown and it results to discontinuously in distance plots. Moreover, Figure 7 provides the heading rate generated, which guides the MAV towards open spaces.

In the second tunnel environment, the MAV autonomously navigates with $z_r = 1.0$ m, $v_{x,r} = 1.2$ m/s, $v_{y,r} = 0.0$ m/s, the Figure 8 shows the distances from the surrounding of the MAV. The dimensions of the second tunnel are smaller, when compared to the first tunnel, however the controller still guarantees a safety distance from all the surface obstacles. Additionally, the generated heading rate command is depicted in Figure 9.

Tunnel Blockage Environment: In this case the MAV navigates through the blockage area, while the constant

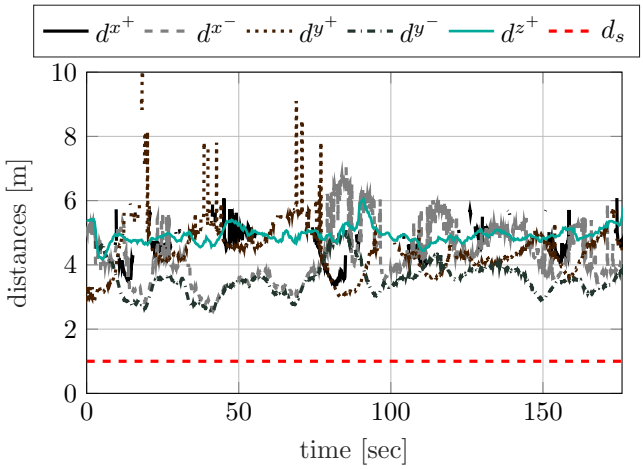

Fig. 6. The distance to the obstacles in x^+, x^-, y^+, y^-, z^+ axes of the MAV, while the safety distance is set to 1 m in the first tunnel environment.

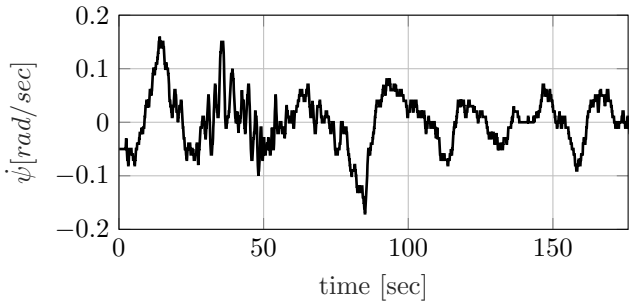

Fig. 7. The heading rate command from the weighted arithmetic mean approach in the first tunnel environment, while the NMPC avoids obstacles.

references of $z_r = 1.0$ m, $v_{x,r} = 0.5$ m/s, $v_{y,r} = 0.0$ m/s are fed to the NMPC. When the MAV reaches the end of the tunnel, the return command is transmitted and the MAV returns to the starting point and passes the blockage again. This test shows the applicability of the method in applications regarding underground mines to navigate in blocked areas and return to the base for the reports. Figure 10 depicts the tunnel blockage environment, where the MAV navigation is evaluated, the altitude reference for the MAV was constant during the experiment, however the MAV passed the blockage successfully.

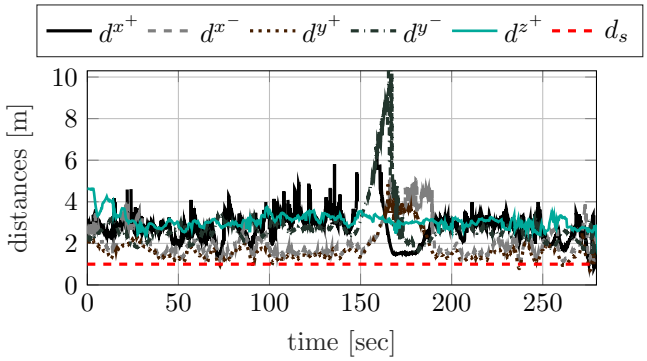

Fig. 8. The distance to the obstacles in x^+, x^-, y^+, y^-, z^+ axes of the MAV, while the safety distance is set to 1 m in the second tunnel environment.

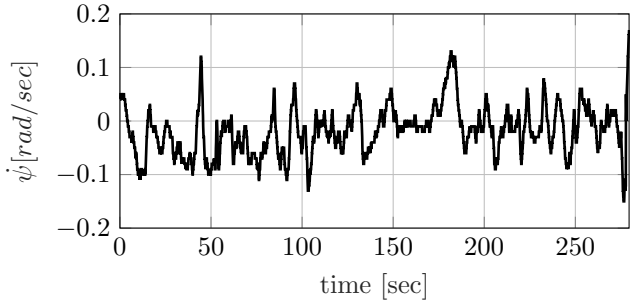

Fig. 9. The heading rate command from a weighted arithmetic mean approach in the case of second tunnel environment navigation, while the NMPC avoids obstacles.

Fig. 10. The tunnel blockage environments, while the MAV navigates autonomously and avoid obstacles.

Figure 11 depicts the distance to obstacles in each axes of the MAV, while the NMPC guarantees safety distance in all directions.

The generated heading rate command is presented in Figure 12, while due to strong magnetic field and disturbances in the IMU, a high peak heading rate command is instantaneously calculated around 42 s as shown in the figure, without affecting the navigation task.

7. CONCLUSIONS

This work presented a MAV navigation scheme, applied in subterranean environments, addressing the challenges of collision avoidance in such harsh environments. The

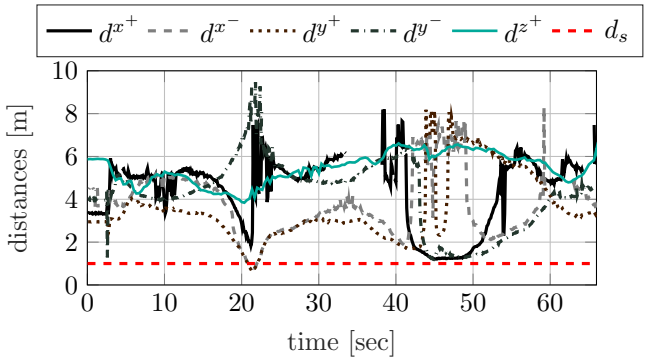

Fig. 11. The distance to the obstacles in x^+, x^-, y^+, y^-, z^+ axes of the MAV, while the safety distance is set to 1 m in the tunnel blockage environment.

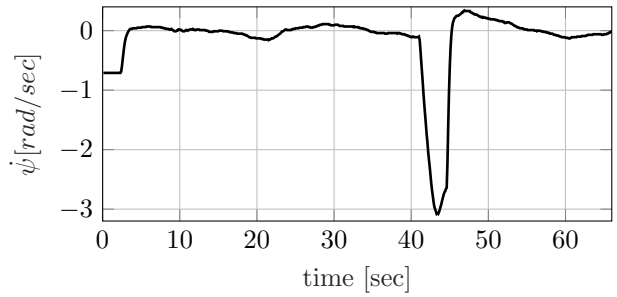

Fig. 12. The heading rate command from the weighted arithmetic mean approach in the tunnel blockage environment navigation, while the NMPC avoids obstacles.

proposed system is developed around a fast NMPC framework, where the MAV is considered as a floating object following velocity references in the $x-y$ plane and position references for the altitude. The NMPC integrates collision avoidance constraints using the kinematics of the obstacles around the MAV, using measurements from Lidar sensors. Moreover, a novel approach for correcting the heading of the MAV towards the center of the mine tunnel is proposed. Experimental trials performed in an underground mine in Sweden demonstrate the performance of the developed navigation method.

REFERENCES

Al-Kaff, A., García, F., Martín, D., De La Escalera, A., and Armingol, J. (2017). Obstacle detection and avoidance system based on monocular camera and size expansion algorithm for uavs. *Sensors*, 17(5), 1061.

Azevedo, F., Oliveira, A., Dias, A., Almeida, J., Moreira, M., Santos, T., Ferreira, A., Martins, A., and Silva, E. (2017). Collision avoidance for safe structure inspection with multirotor uav. In *2017 European Conference on Mobile Robots (ECMR)*, 1–7. IEEE.

Balamurugan, G., Valarmathi, J., and Naidu, V. (2016). Survey on uav navigation in gps denied environments. In *2016 International Conference on Signal Processing, Communication, Power and Embedded System (SCOPES)*, 198–204. IEEE.

Bharadwaj, A., Schultz, A., Gilabert, R., Huff, J., and de Haag, M.U. (2016). Small-uas navigation using 3d imager and infrared camera in structured environments.

In *2016 IEEE/ION Position, Location and Navigation Symposium (PLANS)*, 599–606. IEEE.

Bircher, A., Kamel, M., Alexis, K., Oleynikova, H., and Siegwart, R. (2016). Receding horizon next-best-view planner for 3D exploration. In *IEEE International Conference on Robotics and Automation (ICRA)*, 1462–1468.

Dang, T., Mascarich, F., Khattak, S., Nguyen, H., Khedekar, N., Papachristos, C., and Alexis, K. (2019). Field-hardened robotic autonomy for subterranean exploration. Technical report, EasyChair.

Droeschel, D., Nieuwenhuisen, M., Beul, M., Holz, D., Stückler, J., and Behnke, S. (2016). Multilayered mapping and navigation for autonomous micro aerial vehicles. *Journal of Field Robotics*, 33(4), 451–475.

Hermans, B., Patrinos, P., and Pipeleers, G. (2018). A penalty method based approach for autonomous navigation using nonlinear model predictive control. *IFAC-PapersOnLine*, 51(20), 234 – 240.

Huang, Y.W., Lu, C.L., Chen, K.L., Ser, P.S., Huang, J.T., Shen, Y.C., Chen, P.W., Chang, P.K., Lee, S.C., and Wang, H.C. (2019). Duckiefloat: a collision-tolerant resource-constrained blimp for long-term autonomy in subterranean environments. *arXiv preprint arXiv:1910.14275*.

Kamel, M., Stastny, T., Alexis, K., and Siegwart, R. (2017). Model predictive control for trajectory tracking of unmanned aerial vehicles using robot operating system. In *Robot Operating System (ROS)*, 3–39. Springer.

Kanellakis, C., Mansouri, S.S., Georgoulas, G., and Nikolakopoulos, G. (2018). Towards Autonomous Surveying of Underground Mine Using MAVs. In *International Conference on Robotics in Alpe-Adria Danube Region*, 173–180. Springer.

Lu, Y., Xue, Z., Xia, G.S., and Zhang, L. (2018). A survey on vision-based uav navigation. *Geo-spatial information science*, 21(1), 21–32.

Madansky, A. and Alexander, H. (2017). Weighted standard error and its impact on significance testing. *The Analytical Group, Inc.*

Mansouri, S.S., Arranz, M.C., Kanellakis, C., and Nikolakopoulos, G. (2019). Autonomous MAV navigation in underground mines using darkness contours detection. In *12th International Conference on Computer Vision Systems (ICVS 2019)*.

Mansouri, S.S., Kanellakis, C., Fresk, E., Kominiak, D., and Nikolakopoulos, G. (2018). Cooperative coverage path planning for visual inspection. *Control Engineering Practice*, 74, 118–131.

Mansouri, S.S., Kanellakis, C., Kominiak, D., and Nikolakopoulos, G. (2020). Deploying MAVs for autonomous navigation in dark underground mine environments. *Robotics and Autonomous Systems*, 126, 103472.

Nieuwenhuisen, M. and Behnke, S. (2016). Layered mission and path planning for mav navigation with partial environment knowledge. In *Intelligent Autonomous Systems 13*, 307–319. Springer.

Özaslan, T., Loianno, G., Keller, J., Taylor, C.J., Kumar, V., Wozencraft, J.M., and Hood, T. (2017). Autonomous navigation and mapping for inspection of penstocks and tunnels with MAVs. *IEEE Robotics and Automation Letters*, 2(3), 1740–1747.

Quenzel, J., Nieuwenhuisen, M., Droeschel, D., Beul, M., Houben, S., and Behnke, S. (2019). Autonomous mav-based indoor chimney inspection with 3d laser localization and textured surface reconstruction. *Journal of Intelligent & Robotic Systems*, 93(1-2), 317–335.

Rogers, J.G., Sherrill, R.E., Schang, A., Meadows, S.L., Cox, E.P., Byrne, B., Baran, D.G., Curtis, J.W., and Brink, K.M. (2017). Distributed subterranean exploration and mapping with teams of uavs. In *Ground/Air Multisensor Interoperability, Integration, and Networking for Persistent ISR VIII*, volume 10190, 1019017. International Society for Optics and Photonics.

Sathya, A.S., Sopasakis, P., Van Parys, R., Themelis, A., Pipeleers, G., and Patrinos, P. (2018). Embedded nonlinear model predictive control for obstacle avoidance using panoc. In *Proceedings of the 2018 European Control Conference*.

Shen, S., Michael, N., and Kumar, V. (2012). Stochastic differential equation-based exploration algorithm for autonomous indoor 3D exploration with a micro-aerial vehicle. *The International Journal of Robotics Research*, 31(12), 1431–1444.

Sopasakis, P., Fresk, E., and Patrinos, P. (2020). OpEn: Code generation for embedded nonconvex optimization. In *IFAC World Congress*. Berlin, Germany. URL `http://doc.optimization-engine.xyz/`.